


Article

The Displacement Behaviors of Different Pore-Scales during CO₂ Flooding and Huff-n-Puff Processes in Tight Oil Reservoirs Using Nuclear Magnetic Resonance (NMR)

Mingyang Yang ^{1,*} , Shijun Huang ^{1,*}, Kuiqian Ma ², Fenglan Zhao ¹, Haoyue Sun ¹ and Xinyang Chen ¹¹ School of Petroleum Engineering, China University of Petroleum, Beijing 102249, China² Tianjin Branch of CNOOC Ltd., Tianjin 300459, China

* Correspondence: 15556138068@163.com (M.Y.); hshj@cup.edu.cn (S.H.)

Abstract: Injecting CO₂ into tight oil reservoirs is a potential approach for enhanced oil recovery (EOR) and CO₂ sequestration. However, the effects of different pore-scales on EOR are poorly understood, and this has a significant impact on recovery. In this paper, a pore size correction model based on X-ray computerized tomography (CT) and nuclear magnetic resonance (NMR) was developed in order to establish the relationship between the pore radius and the transverse relaxation time. Different pore-scales are divided according to the cumulative distribution characteristics of the transverse relaxation time (T_2). CO₂ flooding and huff-n-puff experiments were conducted to investigate the dynamic displacement behaviors in different pore-scales. The results indicate that there are three pore-scales: micropores ($T_2 < 0.3$ ms), intermediate pores (0.3 ms $< T_2 < 100$ ms), and macropores (100 ms $< T_2$). However, there are also pseudo-sweep pores (PPs), equilibrium pores (EPs), and sweep pores (SPs) in the intermediate pores, depending on whether crude oil has been produced. Interestingly, the pressurization process causes some crude oil in the large pores to be squeezed into small pores. The recovery of CO₂ huff-n-puff (19.75%) is obviously lower than that of CO₂ flooding (51.61%). Specifically, it was observed that the micropores (−8%) and the pseudo-sweep pores (−37%) have a negative impact on oil recovery, whereas all pore-scales exhibit positive effects during CO₂ flooding. In addition, it was found that the critical pore radiuses of CO₂ flooding and huff-n-puff were 2.61 ms (0.15 μm) and 25 ms (1.5 μm), respectively, in the experiments, and that there is also more oil remaining in the macropores and the sweep pores during CO₂ huff-n-puff. These results provide a deeper understanding of the displacement behaviors of different pore-scales in tight oil reservoirs.



Citation: Yang, M.; Huang, S.; Ma, K.; Zhao, F.; Sun, H.; Chen, X. The Displacement Behaviors of Different Pore-Scales during CO₂ Flooding and Huff-n-Puff Processes in Tight Oil Reservoirs Using Nuclear Magnetic Resonance (NMR). *Processes* **2023**, *11*, 2527. <https://doi.org/10.3390/pr11092527>

Received: 30 June 2023

Revised: 20 August 2023

Accepted: 22 August 2023

Published: 23 August 2023



Copyright: © 2023 by the authors. Licensee MDPI, Basel, Switzerland. This article is an open access article distributed under the terms and conditions of the Creative Commons Attribution (CC BY) license (<https://creativecommons.org/licenses/by/4.0/>).

Keywords: tight oil reservoir; CO₂; NMR; pore-scales; EOR

1. Introduction

Tight oil reservoirs play an increasingly important role in the oil industry due to their great development potential [1–3]. In the last decade, the development of horizontal well and volume fracturing technologies has been of great significance for tight oil production [4,5]. However, the recovery of tight oil reservoirs is usually less than 10 percent of the original oil in place (OOIP) [6]. Therefore, an economic and effective enhanced oil recovery (EOR) method is urgently required. Numerous laboratory experiments and field trials show that CO₂ can significantly improve oil recovery in tight oil reservoirs due to its good injectivity, its viscosity reduction, its lower minimum miscibility pressure (MMP), and its strong ability to both dissolve and expand crude oil [7–9]. Moreover, injecting CO₂ into oil reservoirs is a win–win method, as it can not only produce more oil but also increase CO₂ sequestration [10–12]. At present, the methods for CO₂ injection into reservoirs mainly include CO₂ flooding and huff-n-puff [13–15].

The EOR mechanism of CO₂ huff-n-huff primarily includes dissolved gas drive and diffusion, while convection caused by pressure difference is the main mechanism in the

process of CO₂ flooding. CO₂ huff-n-puff mainly includes three processes: pressuring, soaking, and depletion. During the process of pressuring, convection has a negative impact on EOR [16], and this negative mechanism is often overlooked by researchers. Regarding the second process, diffusion and mass transfer mainly occur during the process of soaking [17,18]. Regarding the third process, similar to primary recovery, a solution gas drive is the main mechanism during the process of depletion [19]. At the same time, the pore size distribution in the reservoir is significant for EOR. CT scanning [20], mercury injection capillary pressure (MICP) [21,22], and NMR [23,24] are all important techniques that are used to characterize the distribution of pore characteristics. CT scanning is also a non-destructive method and favored by many researchers [25,26]. In recent years, there has been increased interest in exploring methods for determining the relationship between pore radius and transverse relaxation time, and these methods can be broadly divided into two types: one is to obtain the conversion coefficient by comparing the peak between the pore radius and the T_2 [27], and the other is to obtain the conversion coefficient by matching the pore radius distribution curve and the T_2 spectral curve [28,29]. However, the pore radius distribution obtained by CT scanning is greatly affected by the resolution. Hence, in this work, the relationship between pore radius and T_2 is obtained by fitting the pore volume distribution curve and the T_2 accumulation curve with different T_2 starting values.

Numerous researchers have conducted extensive studies on the various factors that impact recovery during CO₂ injection [29,30]. Sun et al. quantified the influence of different factors on CO₂ huff-n-puff, and the results showed that the order of importance is CO₂ diffusivity, the number of cycles, injection time, injection rate, and, finally, soaking time [31]. Yu et al. and Ding et al. showed that the lower limit of permeability to CO₂ huff-n-puff is 30 mD [32,33]. Xiang et al. confirmed that CO₂ injection volume is an important factor affecting recovery [34]. However, Ma et al. determined that excessive CO₂ injection may cause lower recovery [35]. Different injection methods have their own advantages and disadvantages. Compared with CO₂ huff-n-puff, CO₂ flooding can achieve higher recovery [36]. However, CO₂ huff-n-puff is a useful and efficient method for solving CO₂ breakthrough, especially for tight oil reservoirs with fractures [37–40]. The size of the pores has a significant impact on recovery, and it is the crude oil within a specific pore space that can be produced [41]. The contribution of different pore sizes to recovery showed that the oil was mainly produced from the macropores in the process of CO₂-EOR [42]. However, the effective pore radius under different CO₂ injection methods is still not properly known. Likewise, the dynamic recovery characteristics of crude oil with different pore sizes during CO₂ huff-n-puff have not been thoroughly studied.

As a case study, monitored use of low-field nuclear magnetic resonance (NMR), CO₂ huff-n-puff, and flooding (10 MPa, 348.15 K) were implemented in order to study the utilization mechanism from a pore-scale perspective in tight oil reservoirs. A pore size correction model based on CT and NMR was built to convert the transverse relaxation time to the pore radius. Different from traditional NMR T_2 distribution analysis, a thorough T_2 cumulative integral distribution analysis was applied in order to identify the different pore-scales, and we also conducted a quantitative evaluation of the different pore-scales on the contribution to recovery. The results of this study will increase understanding of different pore-scale behaviors of CO₂ injection in tight oil reservoirs.

2. Experiments

2.1. Core Samples and Fluids

The oil used in the experiments was obtained from the Changqing Oilfield, Northwest China. The density and the viscosity of the oil were 846.9 kg/m³ and 5.15 mPa.s (at 75 °C and 0.101 Mpa), respectively. The compositional analysis used a gas chromatograph–mass spectrometer of the dead oil, as shown in Figure 1, and it was found that the proportion of intermediate hydrocarbon components in crude oil was high. The CO₂ with a purity of 99.9% that was used in the experiments was obtained from the Huatongjingke Gas Company. The core samples used in the experiments were collected from a tight oil

reservoir: the Changqing Oilfield. The cleaned cores were dried in an oven at 100 °C for 48 h. Then, gas permeability and porosity measurements were conducted in order to study the basic properties of the core samples, which are listed in Table 1.

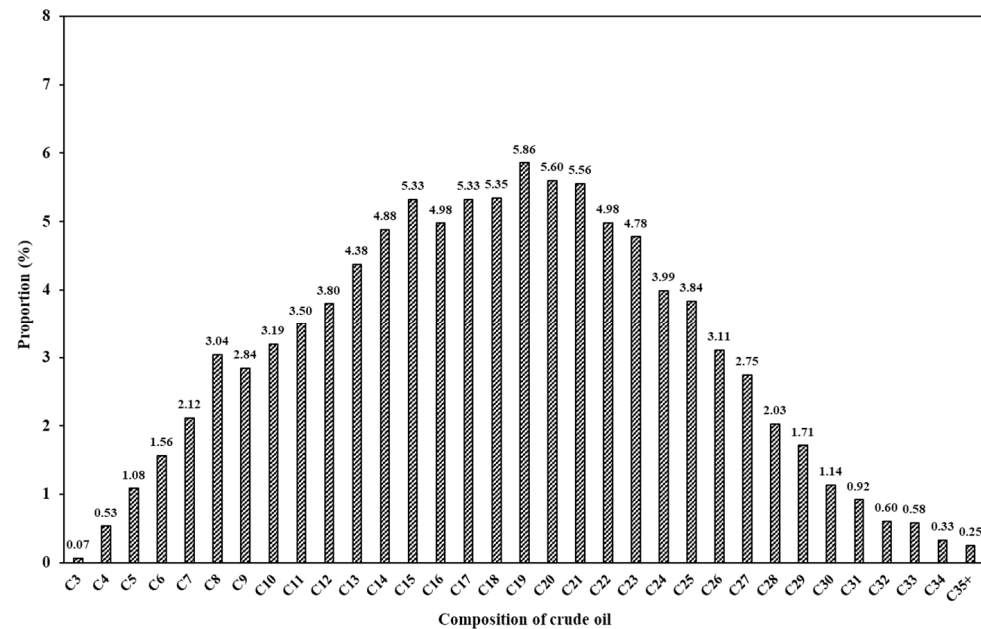


Figure 1. Compositional analysis of the crude oil.

Table 1. The basic properties of core samples used in the experiments.

Core	Length, cm	Diameter, cm	Permeability, mD	Porosity, %	Experiments
#1	7.93	2.51	0.40	15.43	Flooding
#2	8.07	2.50	0.39	15.82	Huff-n-puff

2.2. Experimental Setup

The schematic diagram of the experiment is shown in Figure 2. The main devices include the ISCO pump (Model 100DX, Teledyne CO., Ltd., Thousand Oaks, CA, USA), the core holder, and a low-field NMR measurement system manufactured by Niumag Corporation Ltd. in China. The magnetic field strength and the frequency were 0.22 T and 12 MHz, respectively. Other devices used in the experiments include an incubator, a back pressure pump, a confining pressure pump, intermediate containers, valves, etc. The temperature was set at 348.15 K.

The detailed experimental steps are as follows:

- (1) Sufficient saturation: Place the core into the holder and then set the experimental temperature at 348.15 K. Adjust the injection mode of the pump to a constant speed of 0.1 mL/min. During injection, the confining pressure is 3~5 MPa higher than the upstream displacement pressure. When the oil flows out of the downstream pipeline, increase the back pressure to 10 MPa. Turn off all of the switches and the ISCO pump when the system pressure is stable. Then, the core is aged for 48 h. After this, carry out NMR scanning and 2D nuclear magnetic imaging on rock samples in order to obtain the T2 spectrum curve and 2D crude oil distribution images before CO₂ injection.
- (2) CO₂ flooding: Repeat steps (1) for core sample #1, set back pressure to 10 MPa, set injection speed to 0.1 mL/min, and carry out constant speed CO₂ flooding. When no crude oil is produced at the output end, the experiment is finished. Then, record the final crude oil distribution by NMR.
- (3) CO₂ huff-n-puff: Repeat the steps in (1) for core sample #2. Turn off the downstream switch and set the pump mode to constant pressure 10 MPa injection. When the

- system pressure is stable, close the upstream and downstream switches and then soak for 4 h. Then, slowly turn on the upstream switch. Carry out NMR scanning when no crude oil is produced. Repeat the above steps for 4 cycles.
- (4) Import the relevant data into the NMR analysis system for data analysis.

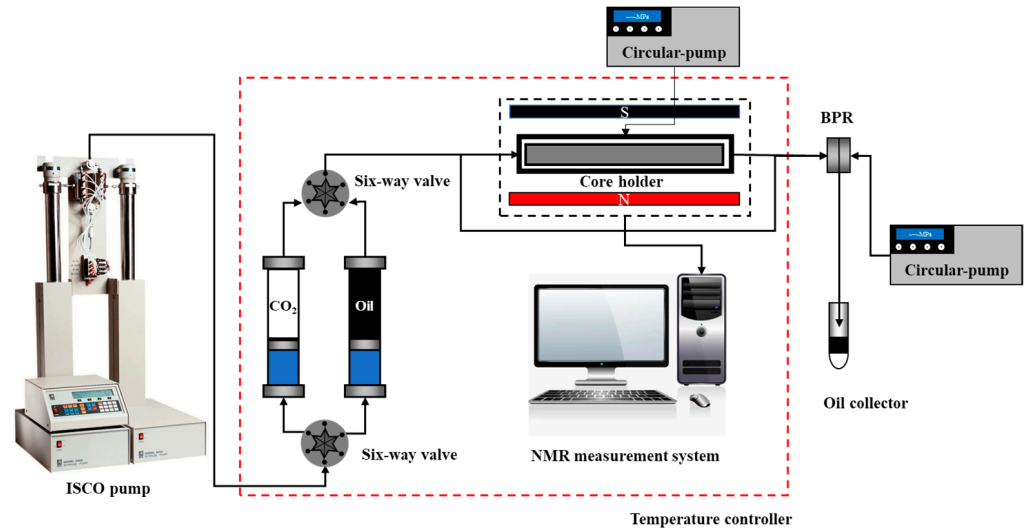


Figure 2. Experimental equipment of CO₂ injection.

2.3. Different Pore-Scale Fitting Correction Model

Here, a pore correction model was built to convert the transverse relaxation time to the pore radius based on the results of the CT and the NMR tests. As shown in Figure 3, we performed CT scanning of core sample #2 in order to obtain the pore characteristics. The results showed that the diameter of the pores is mostly less than 5 μm and that the minimum pore radius that CT scanning can identify is 1.14 μm. Then, the results were statistically analyzed in order to obtain the proportion of different pore sizes, and finally, the cumulative proportion curve of pore sizes was obtained. Although the resolution of the CT scanning needs to be improved, this method has been proven to be effective.

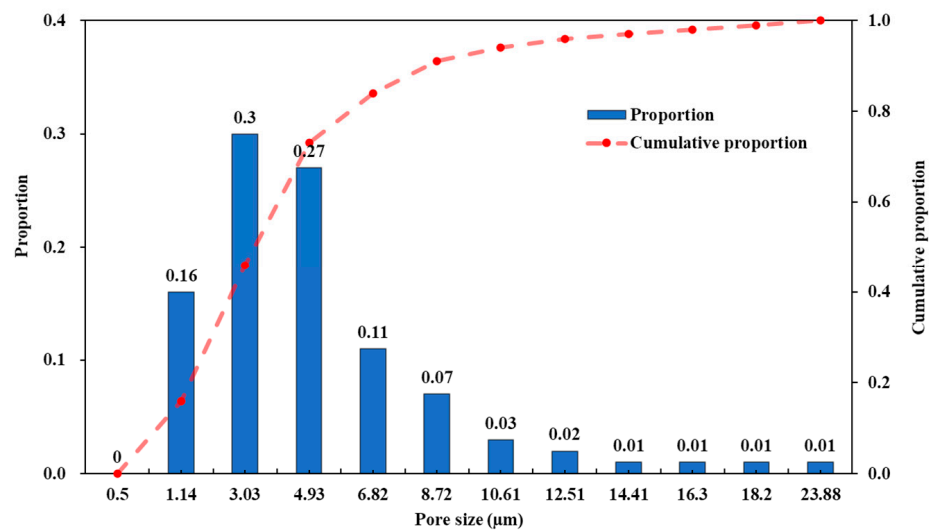


Figure 3. Pore radius distribution of core sample #2.

Transverse relaxation time (T_2) in the NMR tests can be determined by Equation (1) [43]:

$$\frac{1}{T_2} = \frac{1}{T_{2,surface}} + \frac{1}{T_{2,bulk}} + \frac{1}{T_{2,diffusion}} \tag{1}$$

where $T_{2,surface}$, $T_{2,bulk}$, $T_{2,diffusion}$ are the surface relaxation time, the bulk relaxation time, and the diffusion relaxation time, respectively. Because of the uniform magnetic field and the bulk relaxation time are much greater than T_2 , $T_{2,bulk}$ and $T_{2,diffusion}$ are usually neglected. Thus, T_2 can be expressed as follows [44]:

$$T_2 = T_{2,surface} = \frac{V}{\rho_t S} \quad (2)$$

where ρ_t is the surface relaxivity, m/ms; S is the surface area, μm^2 ; and V is the pore volume, μm^3 .

If the pore structure is simplified as a standard spherical structure or a columnar structure, the ratio of the surface area to the volume can be expressed as follows:

$$\frac{S}{V} = \frac{F_s}{r} \quad (3)$$

where F_s is the shape factor of a pore, and r is the pore radius, μm .

Combining Equations (2) and (3), we can obtain the following:

$$T_2 = T_{2,surface} = \frac{r}{\rho_t F_s} = \frac{r}{C_r} \quad (4)$$

where C_r is the conversion coefficient between the pore radius and the relaxation time.

According to Equation (4), the transverse relaxation time is proportional to the pore radius. However, due to the complex pore structure of the rock in the oil reservoirs, it is difficult to measure ρ_t and F_s accurately. We can also obtain the cumulative distribution curve of different pore sizes by CT scanning, but the starting point of the curve is related to the resolution of the CT scanning. We use Q_1 to represent the cumulative distribution function of the pore sizes that were obtained by CT scanning, and we use Q_2 as a function of cumulative amplitude by NMR. The specific relationship is shown in Equations (5) and (6):

$$Q_1 = f_1(r) \quad (5)$$

$$Q_2 = f_2(T_2) \quad (6)$$

where f_1 is the functional relationship between the cumulative distribution and the pore size, and where f_2 is the functional relationship between the cumulative of T_2 spectrum and T_2 . According to $Q_1 = Q_2$, we can deduce the value of C_r , and we can establish the relationship between T_2 and r ($T_2 > 10$ ms).

Figure 4a shows the T_2 spectrum curve of saturated core #2. It is shown that there are two peaks, which indicate the two types of pores in the core sample. The area surrounded by the amplitude and the relaxation time reflects the amount of oil in the pores [45], and the area for the different ranges of T_2 can thereby be obtained. Due to the influence of the resolution, the initial value of the cumulative distribution of the pore sizes obtained by CT scanning is a certain value. Therefore, we need to set the different starting value of the transverse relaxation time, as shown in Figure 4b. According to the fitting results of the pore cumulative distribution curve and the T_2 spectrum cumulative distribution map, the relationship between the pore radius and the relaxation time is obtained, as shown in Figure 5, and the conversion coefficient is 0.059 when T_2 is greater than 10 ms.

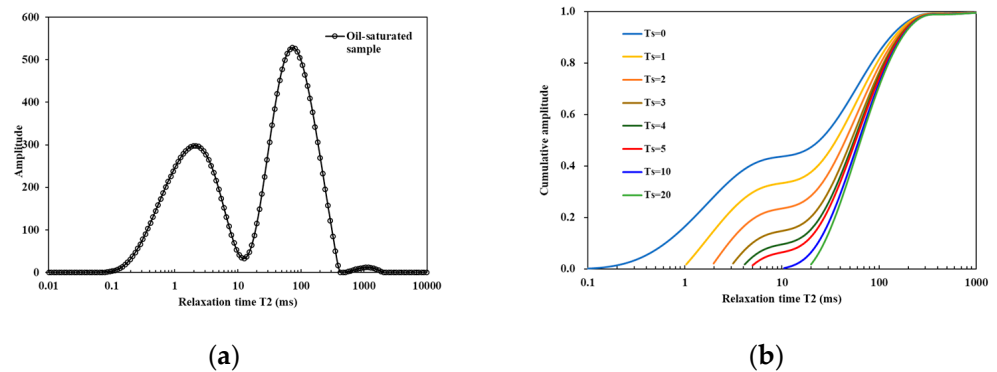


Figure 4. NMR T_2 spectra and cumulative amplitude of the oil-saturated sample #1: (a) T_2 spectra of the core; (b) Cumulative distribution map of T_2 .

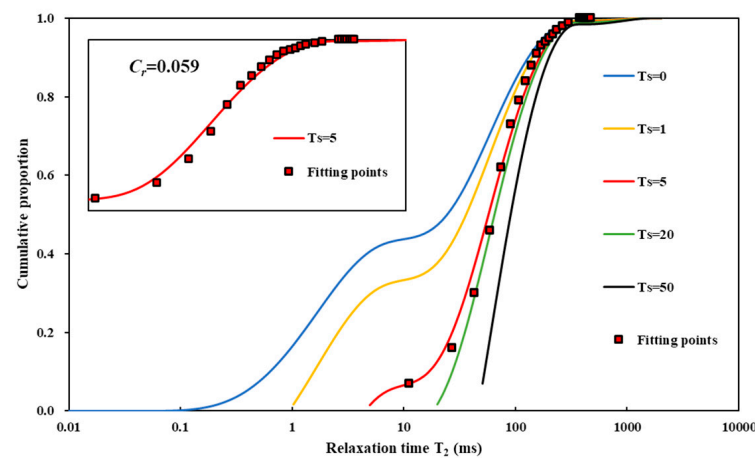


Figure 5. NMR-CT fitting correction model for different pore-scales.

3. Results and Discussion

Pore types are typically classified into micropores and macropores based on the relaxation time of the minimum between the peak values, as shown in Figure 6a. The results show that the crude oil in the macropores is basically completely produced and that the crude oil in the micropores is partially produced during the process of CO_2 flooding, and these results are basically consistent with the conclusions drawn by many scholars [41]. Thus, we can gain a deeper understanding through the integral analysis of the amplitude of the T_2 spectrum. The cumulative amplitude reflects the accumulation of crude oil in the core, which can more clearly distinguish the production of oil in different pore-scales. Figure 6b shows that less crude oil is produced from micropores ($T_2 < 12.6$ ms), while the recovered oil basically comes from macropores. At the same time, the cumulative amplitude after CO_2 displacement is higher than the initial value when $T_2 < 2.61$, and this is due to the increase in pressure during CO_2 injection, which squeezes some of the crude oil in the macropores into the micropores. We call this phenomenon “squeezing”.

Figure 7 shows the 2D images of core sample #1 before and after CO_2 flooding. The amount of crude oil is described by the brightness of the images [46]. Comparing these images, we can find that the remaining oil in the core is fairly non-uniform after CO_2 flooding. The remaining oil is mainly distributed at the end of the core sample, and the recovery is higher at the core inlet. This is probably a consequence of gas breakthrough during CO_2 flooding. We can also see that the sweep volume decreases gradually along the direction of the CO_2 flooding.

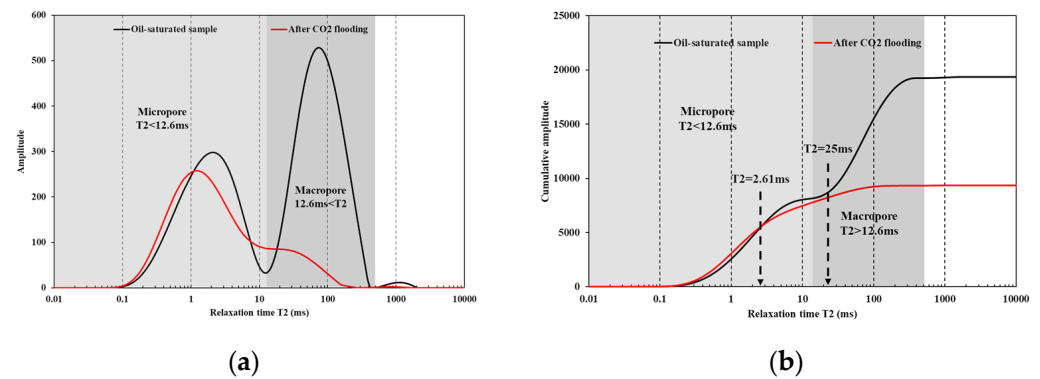


Figure 6. NMR T_2 spectra and cumulative amplitude of the core sample during CO_2 flooding: (a) NMR T_2 spectra of core sample #1; (b) cumulative amplitude of core sample #1.

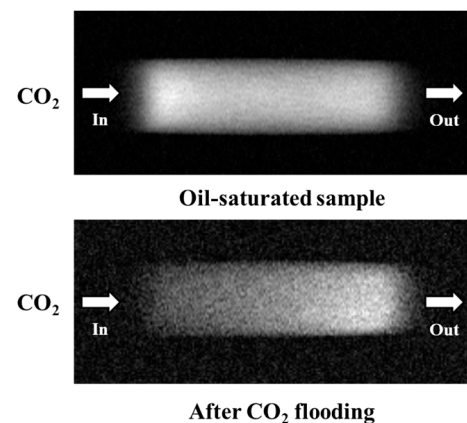


Figure 7. NMR images of the oil saturated sample and after CO_2 flooding.

Figure 8 shows that the crude oil in the macropores and the micropores is gradually recovered during CO_2 huff-n-puff. During the first cycle, the crude oil in different pores was redistributed, and the crude oil in the macropores was then produced. By comparing the T_2 spectral distribution after the first cycle, it is shown that the peaks of the macropores and the micropores gradually shift to the left and down and that the variation in the macropore is larger. This reflects the fact that the crude oil in the macropores is preferentially unlocked during CO_2 huff-n-puff and that the micropores are gradually recovered with the increase in cycles. Overall, the results indicate that the first three cycles usually produced most of the oil in the core [47]. Simultaneously, it can also be observed that the trough amplitude of the T_2 spectral curve increases gradually, primarily due to the fact that the oil in the micropores needs to flow into the large pores. Compared with the injection schemes, the squeezing phenomenon in CO_2 huff-n-puff is more obvious.

Figure 9 shows the recovery of the different cycles and the different pore-scales. The results highlight that the recovery of the four cycles of CO_2 huff-n-puff is 19.75% and that the main contribution of the recovery is produced from the macropores during the first cycle. With the increase in the cycle, the recovery of the macropore gradually decreased. However, it should be noted that micropores still have great potential. The main reason for this is that CO_2 only contacts with micropores through the end face of the core during the early cycles, and CO_2 obtains more opportunities to come into contact with the oil in the micropores when some of the oil in the macropores is recovered [48].

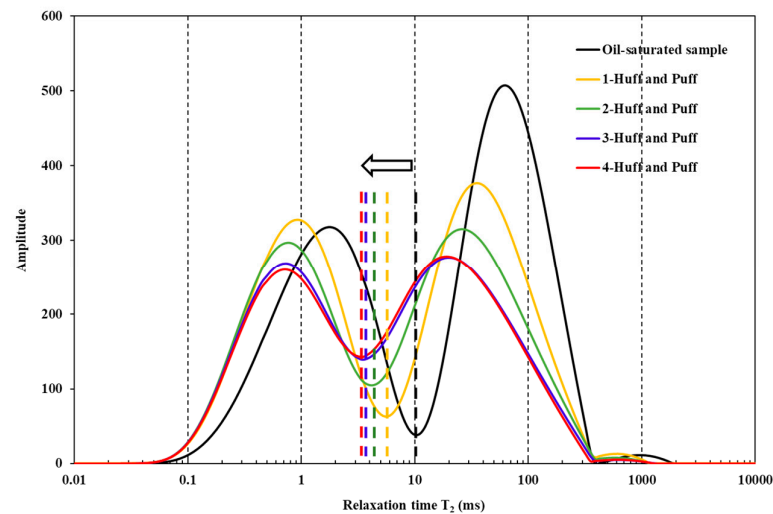


Figure 8. NMR T_2 spectra of the core sample #2 during CO_2 huff-n-puff.

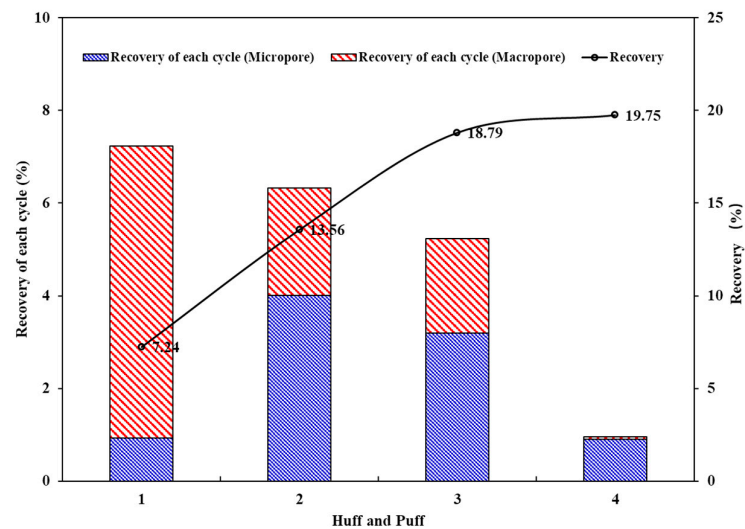


Figure 9. Recovery of each cycle and total recovery.

Figure 10 shows the distribution of the oil at different cycles. During the early stage, the crude oil at the injection end of the core is mainly produced. The remaining oil increases with the distance from the inlet increasing, and this is because the mass transfer and the diffusion between the CO_2 and the crude oil require a long period of time [49]. At the same time, we found that the residual oil at the core inlet increased in the later cycles. During the CO_2 huff-n-puff process, it is worth noting that both CO_2 injection and oil production occur at the same end, which means that the flow of the oil is a countercurrent process. The crude oil flows from the micropores to the macropore by mass transfer, and it then mechanically migrates to the production end. The process of countercurrent leads to some oil accumulating at the injection end.

The cumulative amplitude of different cycles is shown in Figure 11. Based on the distribution of oil at different cycles, the different pores are classified into macropores ($T_2 > 100$ ms), intermediate pores (0.3 ms $< T_2 < 100$ ms), and micropores ($T_2 < 0.3$ ms). Crude oil in the macropores and intermediate pores is produced first, while crude oil in the micropores is basically unrecovered. Interestingly, the intermediate pores are further divided into pseudo-sweep pores (0.3 ms $< T_2 < 10$ ms), equilibrium pores (10 ms $< T_2 < 25$ ms), and sweep pores (25 ms $< T_2 < 100$ ms) according to the effective production of crude oil. The crude oil in sweep pores can be gradually recovered with the increase in the cycles. Under

the process of repeated pressurization, the crude oil in the pseudo-sweep pores cannot be produced effectively. The results indicate that when T_2 is less than 10 ms, the crude oil is basically locked, as indicated in Figure 11.

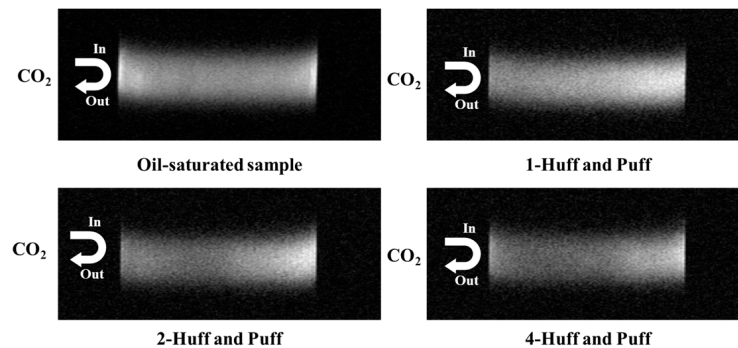


Figure 10. NMR images of the core sample #2 at different cycles.

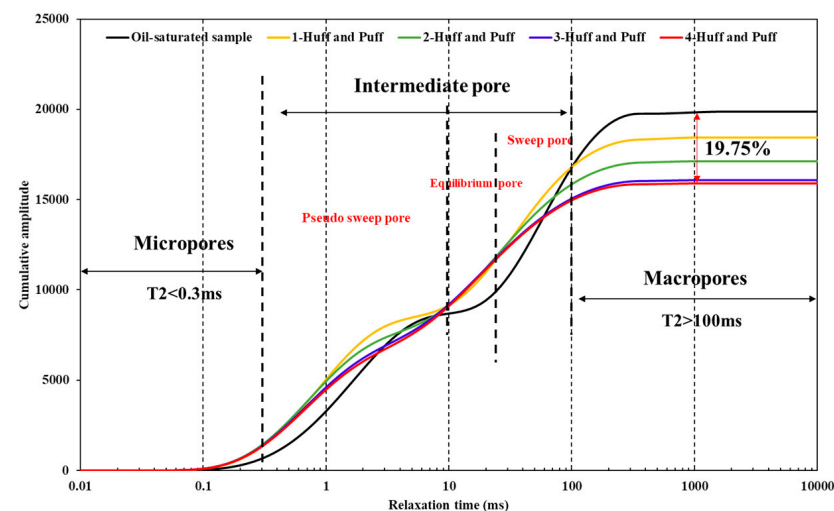


Figure 11. Cumulative amplitude of core sample #2.

The crude oil distribution characteristic in the different pore-scales is shown in Figure 12. Comparing the changes of crude oil in the different pore-scales, it can be found that the micropores and the pseudo-sweep pores occupy a larger pore volume in tight reservoirs, followed by the sweep pores, the macropores, and the equilibrium pores, and the volume of the sweep pores is about twice that of the macropores. With the increase in cycles, the crude oil in the sweep pores and the macropores is gradually produced. However, the oil in the equilibrium pore and the pseudo-sweep pore remains basically unchanged, or even has a tendency to increase. It is possible that some of the crude oil in the larger pores is squeezed into the equilibrium pores during pressurization. Comparing different CO_2 injection schemes, it can be found that more oil is produced from the equilibrium pores, the sweep pores, and the macropores during CO_2 flooding.

Figure 13 shows the contribution of different pore-scales in each cycle during CO_2 huff-n-puff. It is shown that the oil mainly comes from the sweep pores and the macropores and that the contribution of the sweep pores is much higher than that of the macropores, and this is because the sweep pores occupy a larger pore volume in tight reservoirs, as shown in Figure 12. In the first cycle, the negative contribution of the micropore and the equilibrium pore is obvious, and it is -28% and -95% , respectively. The main reason for this is that part of the crude oil in the macropores and the equilibrium pores is squeezed into the smaller pores during pressurization. In the later cycles, the oil in the equilibrium pores and the pseudo-sweep pores exhibits complementary processes. At the same time, we also

found that the contribution of the micropores is 51% in the fourth cycle, which is mainly due to the diffusion and extraction of crude oil in the micropores. The contribution of the macropores decreases first and then increases, while the contribution of the sweep pores decreases gradually, and this is because a small portion of the crude oil in the small pores (i.e., the micropores and the intermediate pores) flows backwards into the macropores.

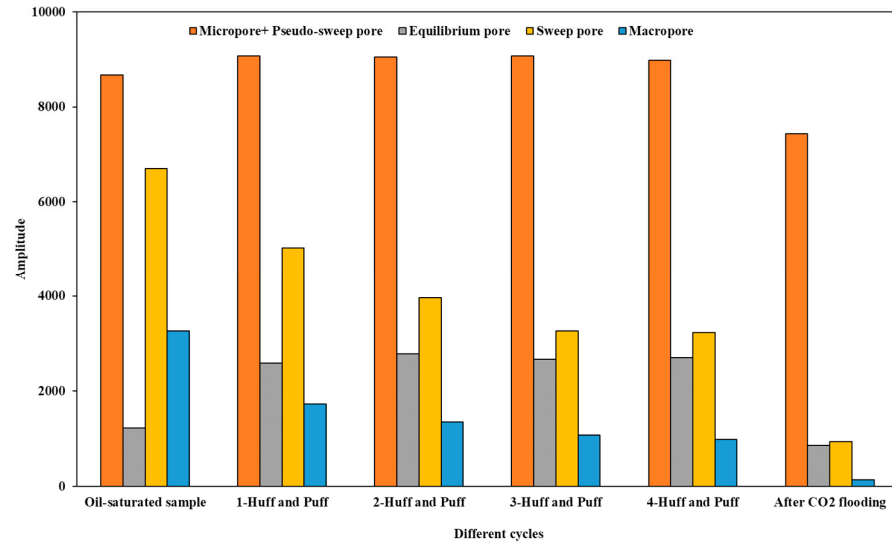


Figure 12. Changes in remaining oil in different pores.

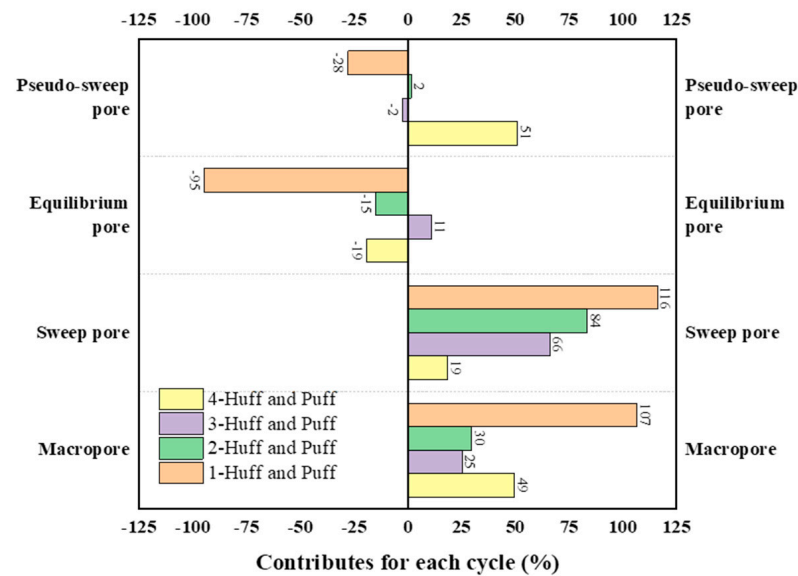


Figure 13. Different pore-scale contributions for each cycle during CO₂ huff-n-puff.

The recovery of CO₂ huff-n-puff is 19.75% while the recovery of CO₂ flooding is 51.61%, as shown in Figure 14. After the first cycle of CO₂ huff-n-puff, the crude oil is redistributed. The lower limits of the pore diameter of the crude oil that is effectively produced by CO₂ huff-n-huff and flooding are 25 ms and 2.61 ms, respectively. The slope of the T₂ spectrum accumulation distribution curve in the late stage of CO₂ huff-n-puff is obviously greater than that of CO₂ flooding ($K_1 > K_2$), which reflects the fact that there is less residual oil after CO₂ flooding. The difference of recovery between CO₂ flooding and huff-n-puff is mainly caused by the equilibrium pores, the sweep pores, and the macropores.

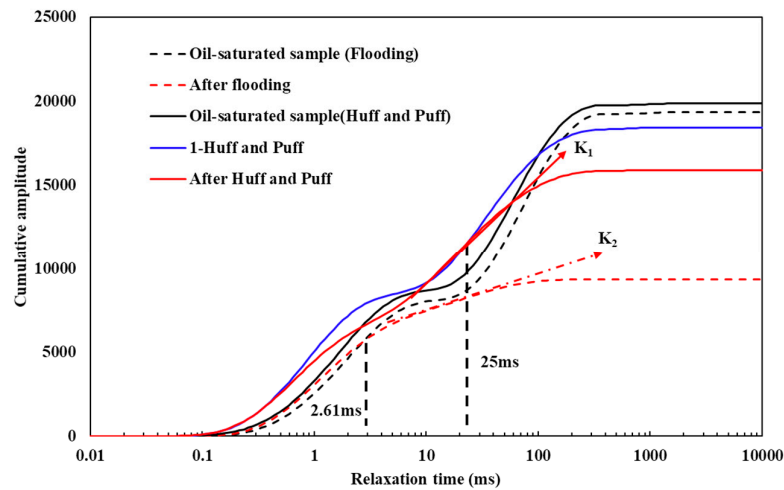


Figure 14. Difference in recovery between CO₂ flooding and huff-n-puff.

Figures 15 and 16 show the contribution and recovery of the different pore-scales examined in this study. Regarding the contribution of the different pore-scales, the results show that the sweep pores and the macropores are the main pores that provide oil. It is worth noting that the contribution of the pseudo-sweep pores and the equilibrium pores under the two injection schemes is different. The results also show that the micropores (−8%) and the equilibrium pores (−37%) both have negative effects on the recovery during CO₂ huff-n-puff, and that the main contribution to the recovery comes from the sweep pores (88%) and the macropores (57%). At the same time, the sweep pores are important for CO₂-EOR and their contribution is higher than that of the macropores, and the main reason for this is that the volume of the sweep pores is about twice that of the macropores, as shown in Figure 12.

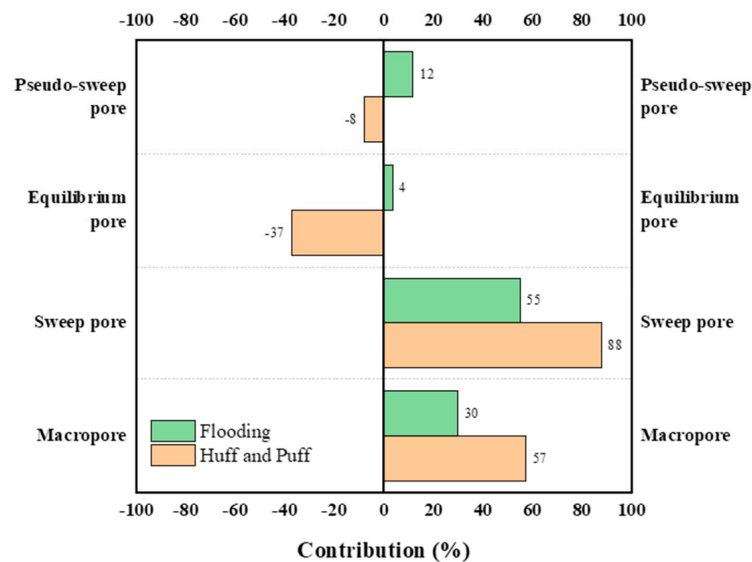


Figure 15. Contribution for different pore-scales with different injection schemes.

Figure 16 shows that the oil in the macropores is mostly recovered (96%) and that most of the crude oil in the sweep pores is recovered (86%) during CO₂ flooding, while only a small part of the crude oil in the equilibrium pores and the pseudo-sweep pores is recovered. Strangely, the recovery of the equilibrium pore was −120%. It can be speculated that part of the oil in the equilibrium pores was recovered during depletion, but due to repeated pressure changes, some of the oil in the macropores was squeezed into the equilibrium pores. At the same time, the pressure increases rapidly in the macropore during the process

of pressurization, which leads to a larger pressure difference between the macropores and the smaller pores (i.e., the intermediate pores and the micropores), and that more crude oil thereby flows into the smaller pores due to the pressure difference. Therefore, the injection pressure during CO₂ huff-n-puff will have a great impact on oil recovery, and we can conclude that the squeeze phenomenon is a significant factor that contributes to the low recovery observed during CO₂ huff-n-puff. At the same time, the accumulation of crude oil caused by the countercurrent cannot be ignored. The EOR mechanism of CO₂ huff-n-puff and flooding is briefly described in Figure 17.

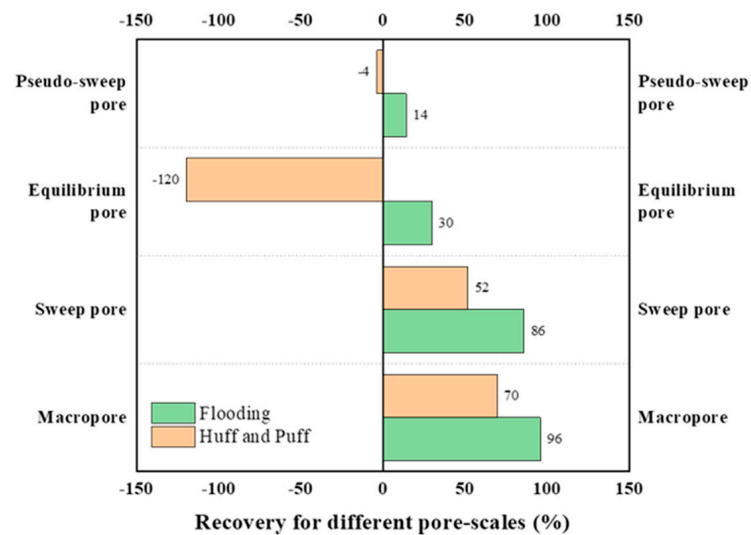


Figure 16. Recovery for different pore-scales with different injection schemes.

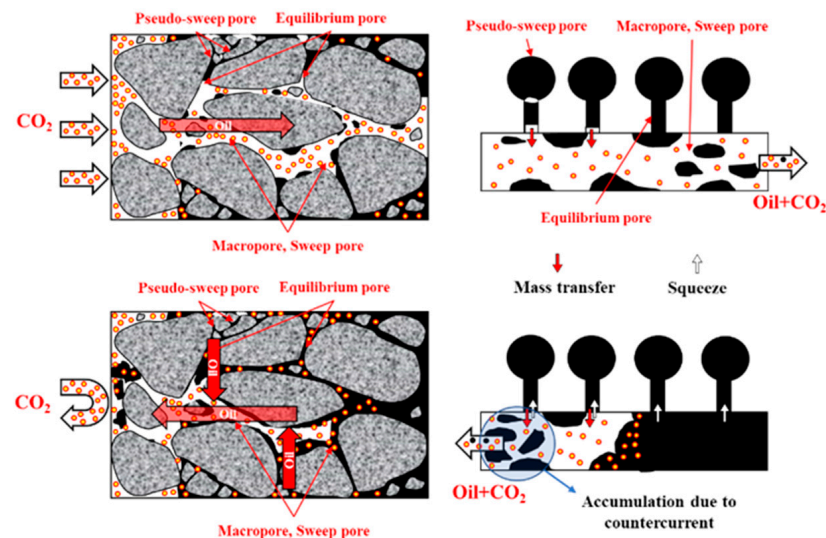


Figure 17. Schematic of the oil recovery mechanisms for CO₂ flooding and huff-n-puff.

4. Conclusions

In this paper, CO₂ flooding and huff-n-puff experiments were carried out in order to understand the recovery of different pore-scales. Based on CT scanning and NMR tests, the relationship between the T_2 spectrum and pore radius was established. According to the cumulative distribution characteristics of the T_2 spectrum, different pore-scales are divided. The recovery and contribution of the different pore-scales was also compared in this paper. Our main conclusions are as follows:

1. The oil recovery of CO₂ flooding and huff-n-puff were 19.75% and 51.61%, respectively. The lower limits of the crude oil effectively produced by CO₂ huff-n-huff and flooding

were 25 ms (1.5 μm) and 2.61 ms (0.15 μm), respectively. The displacement efficiency of CO₂ flooding was higher than that of CO₂ huff-n-huff.

2. According to the distribution of residual oil in different pore sizes, pore types can be divided into macropores, sweep pores, equilibrium pores, pseudo-sweep pores, and micropores. In the process of CO₂ huff-n-puff, the crude oil in the pseudo-sweep pores cannot be effectively recovered, and the crude oil in the sweep pores is gradually produced with the increase in cycles.
3. The contribution of the production mainly comes from the macropores and the sweep pores. Repeated pressurization and depletion during CO₂ huff-n-puff causes the squeezing phenomenon, which has a negative impact on recovery.

In order to fully understand pore-scale displacement behaviors, we will study the influence of different factors on recovery in the future, such as fracture parameters, rock types, and injection and production parameters.

Author Contributions: Methodology, M.Y.; validation, S.H. and K.M.; formal analysis, X.C. and K.M.; investigation, X.C. and H.S.; writing—original draft preparation, M.Y.; supervision, F.Z.; funding acquisition, S.H. and F.Z. All authors have read and agreed to the published version of the manuscript.

Funding: This work was supported by the National Natural Science Foundation of China (52174039) and the National Natural Science Foundation of China (51974328).

Data Availability Statement: The authors confirm that the data supporting the findings of this study are available within the article.

Conflicts of Interest: The authors declare no conflict of interest.

References

1. Alfarge, D.; Wei, M.; Bai, B. CO₂-EOR Mechanisms in Huff-n-Puff Operations in Shale Oil Reservoirs Based on History Matching Results. *Fuel* **2018**, *226*, 112–120. [[CrossRef](#)]
2. Zhou, X.; Yuan, Q.; Zhang, Y.; Wang, H.; Zeng, F.; Zhang, L. Performance Evaluation of CO₂ Flooding Process in Tight Oil Reservoir via Experimental and Numerical Simulation Studies. *Fuel* **2019**, *236*, 730–746. [[CrossRef](#)]
3. Chai, X.; Tian, L.; Zhang, M.; Shao, H.; Wang, J.; Zhang, K. Production Characteristics, Evaluation, and Prediction of CO₂ Water-Alternating-Gas Flooding in Tight Oil Reservoir. *J. Energy Resour. Technol.* **2021**, *144*, 033006. [[CrossRef](#)]
4. Zhang, Y.; Zou, Y.; Zhang, Y.; Wang, L.; Liu, D.; Sun, J.; Ge, H.; Zhou, D. Experimental Study on Characteristics and Mechanisms of Matrix Pressure Transmission near the Fracture Surface during Post-Fracturing Shut-in in Tight Oil Reservoirs. *J. Pet. Sci. Eng.* **2022**, *219*, 111133. [[CrossRef](#)]
5. Saldungaray, P.; Palisch, T.T. *Hydraulic Fracture Optimization in Unconventional Reservoirs*; OnePetro: Richardson, TX, USA, 23 January 2012.
6. Sheng, J.J. Critical Review of Field EOR Projects in Shale and Tight Reservoirs. *J. Pet. Sci. Eng.* **2017**, *159*, 654–665. [[CrossRef](#)]
7. Pu, W.; Wei, B.; Jin, F.; Li, Y.; Jia, H.; Liu, P.; Tang, Z. Experimental Investigation of CO₂ Huff-n-Puff Process for Enhancing Oil Recovery in Tight Reservoirs. *Chem. Eng. Res. Des.* **2016**, *111*, 269–276. [[CrossRef](#)]
8. Li, X.; Xue, J.; Wang, Y.; Yang, W.; Lu, J. Experimental Study of Oil Recovery from Pore of Different Sizes in Tight Sandstone Reservoirs during CO₂ Flooding. *J. Pet. Sci. Eng.* **2022**, *208*, 109740. [[CrossRef](#)]
9. Li, J.; Cui, C.; Wu, Z.; Wang, Z.; Wang, Z.; Yang, H. Study on the Migration Law of CO₂ Miscible Flooding Front and the Quantitative Identification and Characterization of Gas Channeling. *J. Pet. Sci. Eng.* **2022**, *218*, 110970. [[CrossRef](#)]
10. Moh, D.Y.; Zhang, H.; Wang, S.; Yin, X.; Qiao, R. Soaking in CO₂ Huff-n-Puff: A Single-Nanopore Scale Study. *Fuel* **2022**, *308*, 122026. [[CrossRef](#)]
11. Chen, P.; Bose, S.; Selvendran, A.; Thakur, G. Application of CCUS in India: Designing a CO₂ EOR and Storage Pilot in a Mature Field. *Int. J. Greenh. Gas Control* **2023**, *124*, 103858. [[CrossRef](#)]
12. Lv, Q.; Zheng, R.; Zhou, T.; Guo, X.; Wang, W.; Li, J.; Liu, Z. Visualization Study of CO₂-EOR in Carbonate Reservoirs Using 2.5D Heterogeneous Micromodels for CCUS. *Fuel* **2022**, *330*, 125533. [[CrossRef](#)]
13. Hao, Y.; Li, Z.; Su, Y.; Kong, C.; Chen, H.; Meng, Y. Experimental Investigation of CO₂ Storage and Oil Production of Different CO₂ Injection Methods at Pore-Scale and Core-Scale. *Energy* **2022**, *254*, 124349. [[CrossRef](#)]
14. Xiao, P.; Yang, Z.; Wang, X.; Xiao, H.; Wang, X. Experimental Investigation on CO₂ Injection in the Daqing Extra/Ultra-Low Permeability Reservoir. *J. Pet. Sci. Eng.* **2017**, *149*, 765–771. [[CrossRef](#)]
15. Chai, X.; Zhang, M.; Tian, L.; Shi, Z.; Wang, H.; Zhou, Y. Synthetic Model for Evaluating CO₂ Flooding in Tight Oil Reservoir. *Energy Sources Part A Recovery Util. Environ. Eff.* **2021**, 1–12. [[CrossRef](#)]

16. Hydrocarbon Mobilization Mechanisms from Upper, Middle, and Lower Bakken Reservoir Rocks Exposed to CO₂. SPE Canada Unconventional Resources Conference. OnePetro. Available online: <https://onepetro.org/SPEURCC/proceedings/13CURC/All-13CURC/SPE-167200-MS/176764?searchresult=1> (accessed on 20 February 2023).
17. Liu, J.; Li, H.; Tan, Q.; Liu, S.; Zhao, H.; Wang, Z. Quantitative Study of CO₂ Huff-n-Puff Enhanced Oil Recovery in Tight Formation Using Online NMR Technology. *J. Pet. Sci. Eng.* **2022**, *216*, 110688. [[CrossRef](#)]
18. Peng, Z.; Sheng, J. Diffusion Effect on Shale Oil Recovery by CO₂ Huff-n-Puff. *Energy Fuels* **2023**, *37*, 2774–2790. [[CrossRef](#)]
19. Li, L.; Su, Y.; Hao, Y.; Zhan, S.; Lv, Y.; Zhao, Q.; Wang, H. A Comparative Study of CO₂ and N₂ Huff-n-Puff EOR Performance in Shale Oil Production. *J. Pet. Sci. Eng.* **2019**, *181*, 106174. [[CrossRef](#)]
20. Wu, Y.; Lin, C.; Ren, L.; Yan, W.; An, S.; Chen, B.; Wang, Y.; Zhang, X.; You, C.; Zhang, Y. Reconstruction of 3D Porous Media Using Multiple-Point Statistics Based on a 3D Training Image. *J. Nat. Gas Sci. Eng.* **2018**, *51*, 129–140. [[CrossRef](#)]
21. Lai, J.; Wang, G.; Cao, J.; Xiao, C.; Wang, S.; Pang, X.; Dai, Q.; He, Z.; Fan, X.; Yang, L.; et al. Investigation of Pore Structure and Petrophysical Property in Tight Sandstones. *Mar. Pet. Geol.* **2018**, *91*, 179–189. [[CrossRef](#)]
22. Okolo, G.N.; Everson, R.C.; Neomagus, H.W.J.P.; Roberts, M.J.; Sakurovs, R. Comparing the Porosity and Surface Areas of Coal as Measured by Gas Adsorption, Mercury Intrusion and SAXS Techniques. *Fuel* **2015**, *141*, 293–304. [[CrossRef](#)]
23. Li, J.; Yin, J.; Zhang, Y.; Lu, S.; Wang, W.; Li, J.; Chen, F.; Meng, Y. A Comparison of Experimental Methods for Describing Shale Pore Features—A Case Study in the Bohai Bay Basin of Eastern China. *Int. J. Coal Geol.* **2015**, *152*, 39–49. [[CrossRef](#)]
24. Stallmach, F.; Vogt, C.; Kärger, J.; Helbig, K.; Jacobs, F. Fractal Geometry of Surface Areas of Sand Grains Probed by Pulsed Field Gradient NMR. *Phys. Rev. Lett.* **2002**, *88*, 105505. [[CrossRef](#)] [[PubMed](#)]
25. Wu, Y.; Tahmasebi, P.; Lin, C.; Zahid, M.A.; Dong, C.; Golab, A.N.; Ren, L. A Comprehensive Study on Geometric, Topological and Fractal Characterizations of Pore Systems in Low-Permeability Reservoirs Based on SEM, MICP, NMR, and X-ray CT Experiments. *Mar. Pet. Geol.* **2019**, *103*, 12–28. [[CrossRef](#)]
26. Zhao, Y.; Zhu, G.; Dong, Y.; Danesh, N.N.; Chen, Z.; Zhang, T. Comparison of Low-Field NMR and Microfocus X-ray Computed Tomography in Fractal Characterization of Pores in Artificial Cores. *Fuel* **2017**, *210*, 217–226. [[CrossRef](#)]
27. Zhao, J.; Wang, P.; Yang, H.; Tang, F.; Ju, Y.; Jia, Y. Experimental Investigation of the CO₂ Huff and Puff Effect in Low-Permeability Sandstones with NMR. *ACS Omega* **2021**, *6*, 15601–15607. [[CrossRef](#)] [[PubMed](#)]
28. Yao, Y.; Liu, D.; Che, Y.; Tang, D.; Tang, S.; Huang, W. Petrophysical Characterization of Coals by Low-Field Nuclear Magnetic Resonance (NMR). *Fuel* **2010**, *89*, 1371–1380. [[CrossRef](#)]
29. Gao, H.; Pu, W. Experimental Study on Supercritical CO₂ Huff and Puff in Tight Conglomerate Reservoirs. *ACS Omega* **2021**, *6*, 24545–24552. [[CrossRef](#)]
30. Li, T.; Gao, H.; Ni, J.; Wang, C.; Cheng, Z.; Xue, J.; Luo, K. Research on the Differential Oil Producing in the Various Scale Pores under Different CO₂ Flooding Modes with a Fluid Distribution Pore Classification Method. *Energy Fuels* **2023**, *37*, 3775–3784. [[CrossRef](#)]
31. Sun, R.; Yu, W.; Xu, F.; Pu, H.; Miao, J. Compositional Simulation of CO₂ Huff-n-Puff Process in Middle Bakken Tight Oil Reservoirs with Hydraulic Fractures. *Fuel* **2019**, *236*, 1446–1457. [[CrossRef](#)]
32. Ding, M.; Wang, Y.; Liu, D.; Wang, X.; Zhao, H.; Chen, W. Enhancing Tight Oil Recovery Using CO₂ Huff and Puff Injection: An Experimental Study of the Influencing Factors. *J. Nat. Gas Sci. Eng.* **2021**, *90*, 103931. [[CrossRef](#)]
33. Zuloaga, P.; Yu, W.; Miao, J.; Sepehrnoori, K. Performance Evaluation of CO₂ Huff-n-Puff and Continuous CO₂ Injection in Tight Oil Reservoirs. *Energy* **2017**, *134*, 181–192. [[CrossRef](#)]
34. Tang, X.; Li, Y.; Han, X.; Zhou, Y.; Zhan, J.; Xu, M.; Zhou, R.; Cui, K.; Chen, X.; Wang, L. Dynamic Characteristics and Influencing Factors of CO₂ Huff and Puff in Tight Oil Reservoirs. *Pet. Explor. Dev.* **2021**, *48*, 946–955. [[CrossRef](#)]
35. Ma, J.; Wang, X.; Gao, R.; Zeng, F.; Huang, C.; Tontiwachwuthikul, P.; Liang, Z. Enhanced Light Oil Recovery from Tight Formations through CO₂ Huff 'n' Puff Processes. *Fuel* **2015**, *154*, 35–44. [[CrossRef](#)]
36. Wang, X.; Luo, P.; Er, V.; Huang, S. *Assessment of CO₂ Flooding Potential for Bakken Formation, Saskatchewan*; OnePetro: Richardson, TX, USA, 19 October 2010.
37. Du, D.; Pu, W.; Jin, F.; Liu, R. Experimental Study on EOR by CO₂ Huff-n-Puff and CO₂ Flooding in Tight Conglomerate Reservoirs with Pore Scale. *Chem. Eng. Res. Des.* **2020**, *156*, 425–432. [[CrossRef](#)]
38. Wang, X.-W.; Xiao, P.; Yang, Z.-M.; Liu, X.-W.; Xia, Z.-Z.; Wang, L.-Q. Laboratory and Field-Scale Parameter Optimization of CO₂ Huff-n-Puff with the Staged-Fracturing Horizontal Well in Tight Oil Reservoirs. *J. Pet. Sci. Eng.* **2020**, *186*, 106703. [[CrossRef](#)]
39. Li, D.; Saraji, S.; Jiao, Z.; Zhang, Y. CO₂ Injection Strategies for Enhanced Oil Recovery and Geological Sequestration in a Tight Reservoir: An Experimental Study. *Fuel* **2021**, *284*, 119013. [[CrossRef](#)]
40. Hawthorne, S.B.; Gorecki, C.D.; Sorensen, J.A.; Miller, D.J.; Harju, J.A.; Melzer, L.S. Hydrocarbon Mobilization Mechanisms Using CO₂ in an Unconventional Oil Play. *Energy Procedia* **2014**, *63*, 7717–7723. [[CrossRef](#)]
41. Wan, T.; Wang, W.; Jiang, J.; Zhang, Y. Pore-Scale Analysis of Gas Huff-n-Puff Enhanced Oil Recovery and Waterflooding Process. *Fuel* **2018**, *215*, 561–571. [[CrossRef](#)]
42. Wei, B.; Zhang, X.; Wu, R.; Zou, P.; Gao, K.; Xu, X.; Pu, W.; Wood, C. Pore-Scale Monitoring of CO₂ and N₂ Flooding Processes in a Tight Formation under Reservoir Conditions Using Nuclear Magnetic Resonance (NMR): A Case Study. *Fuel* **2019**, *246*, 34–41. [[CrossRef](#)]

43. Dong, X.; Shen, L.W.; Liu, X.; Zhang, P.; Sun, Y.; Yan, W.; Jiang, L.; Wang, F.; Sun, J. NMR Characterization of a Tight Sand's Pore Structures and Fluid Mobility: An Experimental Investigation for CO₂ EOR Potential. *Mar. Pet. Geol.* **2020**, *118*, 104460. [[CrossRef](#)]
44. Liu, Y.; Yao, Y.; Liu, D.; Zheng, S.; Sun, G.; Chang, Y. Shale Pore Size Classification: An NMR Fluid Typing Method. *Mar. Pet. Geol.* **2018**, *96*, 591–601. [[CrossRef](#)]
45. Liu, J.; Sheng, J.J. Experimental Investigation of Surfactant Enhanced Spontaneous Imbibition in Chinese Shale Oil Reservoirs Using NMR Tests. *J. Ind. Eng. Chem.* **2019**, *72*, 414–422. [[CrossRef](#)]
46. Chen, T.; Yang, Z.; Ding, Y.; Luo, Y.; Qi, D.; Lin, W.; Zhao, X. Waterflooding Huff-n-Puff in Tight Oil Cores Using Online Nuclear Magnetic Resonance. *Energies* **2018**, *11*, 1524. [[CrossRef](#)]
47. Li, S.; Sun, L.; Wang, L.; Li, Z.; Zhang, K. Hybrid CO₂-N₂ Huff-n-Puff Strategy in Unlocking Tight Oil Reservoirs. *Fuel* **2022**, *309*, 122198. [[CrossRef](#)]
48. Chen, H.; Yang, M.; Huang, C.; Wang, Y.; Zhang, Y.; Zuo, M. A Dynamic Model of CO₂ Diffusion Coefficient in Shale Based on the Whole Process Fitting. *Chem. Eng. J.* **2022**, *428*, 131151. [[CrossRef](#)]
49. Du, D.; Li, C.; Song, X.; Liu, Q.; Ma, N.; Wang, X.; Shen, Y.; Li, Y. Experimental Study on Residue Oil Distribution after the Supercritical CO₂ Huff-n-Puff Process in Low Permeability Cores with Nuclear Magnetic Resonance (NMR). *Arab. J. Chem.* **2021**, *14*, 103355. [[CrossRef](#)]

Disclaimer/Publisher's Note: The statements, opinions and data contained in all publications are solely those of the individual author(s) and contributor(s) and not of MDPI and/or the editor(s). MDPI and/or the editor(s) disclaim responsibility for any injury to people or property resulting from any ideas, methods, instructions or products referred to in the content.